Journal of Power Sources 226 (2013) 191–201

Contents lists available at SciVerse ScienceDirect

Journal of Power Sources

journal homepage: www.elsevier.com/locate/jpowsour

Evaluation of UltraBattery™ performance in comparison with a battery-supercapacitor parallel network

A.J. Fairweather [a,*], D.A. Stone [b], M.P. Foster [b]

[a] VxI Power Ltd, Lincoln, UK
[b] Department of Electrical and Electronic Engineering, The University of Sheffield, UK

HIGHLIGHTS

- ► Comparative electrical performance of an ultra battery and a lead-acid battery is examined.
- ► A model is developed for the ultra battery which is verified experimentally.
- ► Comparisons are made to conventional lead-acid battery/supercapacitor parallel networks.
- ► Parallel network tests highlight the respective roles of the supercapacitor and battery.
- ► The work informs application of the ultra battery to transient charge/discharge applications.

ARTICLE INFO

Article history:
Received 25 August 2012
Received in revised form
12 October 2012
Accepted 15 October 2012
Available online 8 November 2012

Keywords:
Batteries
Supercapacitors
PRBS
Parameter estimation
Impedance spectroscopy

ABSTRACT

This paper examines the emerging technology of batteries incorporating carbon in the negative plate to affect a parallel capacitance within the battery itself. Using a frequency domain approach in conjunction with low frequency static tests and step responses an UltraBattery™ is examined. Initial examinations using the Randles' model lead to development of a modified model to better represent the battery parameters. These findings then expand the work to examine a similar conventional battery connected in a parallel network with a supercapacitor bank, allowing comparisons to be made and performance criteria to be established.

1. Introduction

Battery applications remain an area of rapid growth as transitions in motive power from fossil fuels to electricity continue. The growth of hybrid and full-electric vehicles continues as nations seek to meet internationally agreed emission targets. Battery technologies and chemistries are in a phase of development which reflects these new applications, with many vehicle applications adopting lithium chemistries as the standard for energy storage. Lead-acid batteries do however have a role to play in the future of storage technologies, being attractive in terms of a mature and well understood recycling infrastructure, and generally impart a much lower cost of ownership than their more exotic counterparts. With this in mind, performance improvements continue to be sought for this chemistry, and much focus is placed on reducing the effects of high discharge rate, current acceptance and delivery during rapid transitions between charge and discharge conditions. Supercapacitors are an attractive prospect in storage applications due to the fact the major issues with batteries are not applicable, however, the energy density of supercapacitors still remains too low to completely supplant batteries, so a mix of the two technologies remains a desirable prospect.

1.1. Performance limitations of lead-acid batteries

As has already been mentioned batteries suffer performance limitations when used in applications where the charge and discharge profiles present themselves as high frequency ripple currents. Moving from a state of charge to discharge in a lead-acid

* Corresponding author.
E-mail addresses: andrew.fairweather@vxipower.com (A.J. Fairweather), D.A.Stone@sheffield.ac.uk (D.A. Stone), m.p.foster@sheffield.ac.uk (M.P. Foster).

0378-7753/$ – see front matter © 2012 Elsevier B.V. All rights reserved.
http://dx.doi.org/10.1016/j.jpowsour.2012.10.095

Nomenclature

c	rated capacity, Ah
C	capacitance, F
C_{Bulk}	bulk capacitive element of cell, F
C_p	Peukert capacity, Ah
$C_{Surface}$	double layer capacitance, F
I	current, A
K	Peukert coefficient, –
Q	electrical charge, C
R_d	self-discharge resistance, Ω
R_i	series resistive element (Randle's circuit), Ω
R_t	charge transfer resistance, Ω
T	time, s
V_{EOD}	end-of-discharge voltage, V
V_{OCT}	open-circuit-terminal voltage, V
WC_{Bulk}	energy stored within bulk capacitor, J
τ	time constant, s

battery requires chemical processes to occur which in themselves give rise to voltage drops as these reactions proceed.

In (1) we can see the charge and discharge reactions. If charge to the battery is removed and a discharge immediately applied there is a defined time for this transition to occur, which will depend upon factors such as temperature, state of health, and state of charge of the subject battery.

$$Pb + PbO_2 + 2H_2SO_4 \overset{\text{Discharge}}{\underset{\text{charge}}{\rightleftharpoons}} 2PbSO_4 + 2H_2O \quad (1)$$

Furthermore, the effect of increased discharge current is well known from the work of Peukert [1] who described the reduction in effective capacity of lead-acid cells with discharge rate:

$$C_p = I^k t \quad (2)$$

where C_p is capacity according to Peukert, at a specified discharge rate.

I is discharge current in Amperes
k is the Peukert constant for the battery
t is the time of discharge in hours

These factors seriously affect both the performance and service life of lead-acid cells used in transient mode current applications.

1.2. Capacitors and batteries

In order to understand the relative benefits of different energy storage devices, an understanding of the modes of storage is required.

The way in which batteries and capacitors store energy is fundamentally different. Batteries store electrical energy indirectly as potential chemical energy. To release this energy oxidation and reduction reactions occur (equation (1)) which allows charges to be released facilitating electrical work when these flow between two electrodes at different potentials. In contrast, capacitors store energy directly in an electrostatic way, as negative and positive charges on the plates of a capacitor, a process known as non-Faradaic energy storage.

It therefore follows that batteries, with a technology which is based on chemical reactions, will have response times and performance based on the basic controlling criteria for speed of chemical reactions (concentration of reactant, temperature, and addition of catalysts). Moves to increase reaction speeds within batteries to improve performance have a negative downside, as faster reaction times for the desirable reactions cannot readily be separated from those which shorten battery life (plate corrosion etc.), so as a means to improve battery performance, these measures are generally avoided.

In contrast, capacitors undergo no electrochemical reactions in their conversion of stored charge to electrical energy, and vice versa. The implications of this are two-fold: Firstly, the conversion of stored charge to electrical energy is rapid, and charge can be affected in a similarly brisk fashion.

Secondly, within batteries, the chemical inter-conversions of the anode and cathode materials in the cell take place with phase changes, and some irreversibility of the conversion of the anode and cathode reactive materials occurs. This leads to the limitations on cycle life experienced by batteries (1000–1500 cycles typically). Because these processes do not exist within capacitors, 10^5–10^6 cycles are commonplace [2].

The main disadvantage with capacitors however is energy density. At the molecular level, limitations exist which restrict this energy in capacitors to 20% of that of batteries of similar active area [2], and conventional capacitor technologies exploit a small proportion of this. However, with the development of electrochemical supercapacitors active area utilisation has improved, allowing the complementary characteristics of the two energy storage technologies to be more adequately exploited.

1.3. Supercapacitors

Capacitors traditionally have found applications in short term energy storage applications, with capacitance values rarely surpassing 1 F. High value capacitors were subsequently developed and used as alternatives to small lithium cells in memory retention applications. Further development in this area has led to the high value supercapacitors we see today being employed in a range of applications from wind turbines [3] to uninterruptable power supplies [4]. Supercapacitors, or electrochemical capacitors differ in some respects from traditional capacitors in that they do not employ a conventional dielectric. High-area porous materials are used in a very thin layer that facilitates a large double layer capacitance. The thin dielectric does however lead to the low working voltage of these capacitors generally, often requiring series connection in application.

1.4. High-carbon batteries

"High-carbon" has become a generally adopted term for batteries and cells employing carbon in the negative plate to improve performance. Carbon is a high-area material and is widely employed throughout the Engineering disciplines for its catalytic and absorption properties [5,6]. It is increasingly utilised within energy storage technologies as a means to increase charge acceptance [7] and improve performance generally [8,9]. Lead-acid cells comprise a positive and negative plate, consisting of lead dioxide and sponge lead respectively. Developments in carbon enhanced negative plates have led to the development of asymmetric supercapacitors using the conventional positive plate with a carbon based negative plate. Connecting these different cell configurations in parallel leads to a battery with integral capacitance which is suitable for HEV duty [10–12].

1.5. Battery models

In order to facilitate analysis of battery performance, suitable models are adopted in order to provide representations of the subject batteries. Within this work, the familiar Randles' model was used for the battery (Fig. 1). This model is a simple electrical representation of the complex electrochemical processes, with lumped parameters representing the cell. It assumes the conditions for charge and discharge of the cell are the same, and does not take into account charge inefficiency. It is, however, a usable electrical analogy to the chemical processes of the cell.

R_i is the lumped resistance for the cell interconnections etc. and represents the major series resistance for the cell. $C_{Surface}$ is a double layer capacitance, which is a result of the charge separation at the interface between the electrolyte and the cell plate [13]. R_t, connected in parallel with the double layer capacitance, is the charge transfer resistance. This property is the electrical analogy of the inherent speed of the charge transfer reaction.

C_{Bulk} represents the dominant capacitive element of the cell and R_d is the self-discharge resistance of the cell, shown as a load across the bulk element of capacitance, typically high (>10 kΩ) for a healthy cell.

Examination of the UltraBattery™ leads to a modified model based on the additional capacitance connected in parallel with the battery itself. The model shown in Fig. 2 was adopted for its applicability to both the UltraBattery™ and the conventional battery/supercapacitor parallel combination.

2. Cell parameter estimation

Analysis of batteries and cells by electrical means can be carried out by several approaches. Amongst these, traditionally, discharge tests and responses to pulse loads have been widely used in order to arrive at values for the Randles' model.

AC impedance testing has been also widely employed within this field [14], however using a spot frequency tends to reveal a bulk impedance value, and although this remains usable as a pass/fail test for standby batteries in application, an expansion of the techniques is required if more detailed information is required. Swept frequency analysis allows an impedance response over frequency range for the battery or cell under test. This method can, however, be laborious, so a more suitable frequency rich excitation signal which allows time-efficient testing and data analysis can be adopted. Within this work, a combination of discharge testing, pulse testing and a frequency domain approach using signals of appropriate spectral content is described.

2.1. Discharge testing

Battery or cell capacity can most readily be established by discharge testing. The published capacity for a given battery will be related to a specific discharge rate. The end-of-discharge voltage

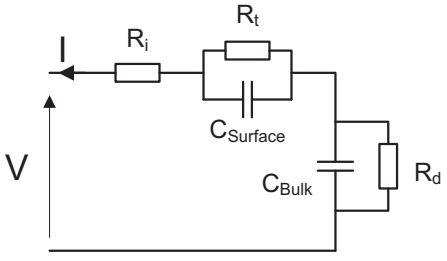

Fig. 1. Randles' equivalent circuit.

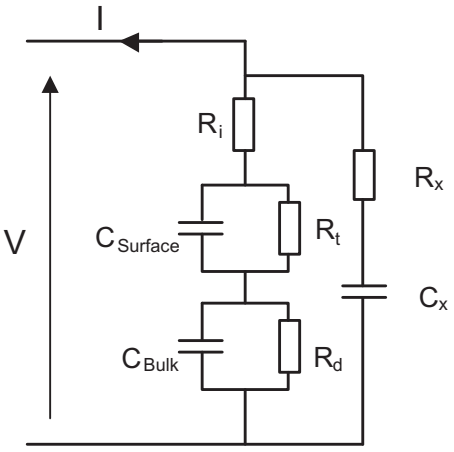

Fig. 2. Modified Randles' model for the UltraBattery™.

(V_{EOD}) for this discharge rate will be stated by the manufacturer, beyond which irreversible capacity loss occurs, and the battery will be permanently damaged. The majority of VRLA batteries are rated at a 20 h discharge rate, usually quoted as a factor of overall capacity, i.e. 0.05 C for 20 h, for which a V_{EOD} of around 2 V/cell 20 °C will apply.

Initial estimates of the capacitance of a battery can be made before verification by experiment, based on estimated open-circuit-terminal (V_{OCT}) and end-of-discharge (V_{EOD}) voltages [15].

$$W_{C_{Bulk}} = \frac{1}{2} C_{bulk}\left(V^2\right) \tag{3}$$

$$= \frac{1}{2} C_{bulk}\left(V_{100\%SOC}^2 - V_{0\%SOC}^2\right) \tag{4}$$

And therefore,

$$C_{Bulk\ Initial} = \frac{\text{Rated capacity} \times V_{100\%SOC}}{\frac{1}{2}\left(V_{100\%SOC}^2 - V_{0\%SOC}^2\right)} \tag{5}$$

2.2. Pulse testing

Application of load pulses to batteries and cells can reveal much about the equivalent circuit, but is most appropriate to the medium to high frequencies of interest within the battery.

Combinations of constant current load, followed by short off-load transitions, and specific load pulses lead to identification of equivalent circuit parameters. Such schemes are implemented commercially, and can be used to report state of health (SoH) [16]. Using a battery or cell response to an off-load transient the remaining Randles' circuit parameters can be identified [15,17].

2.3. Pseudo random binary sequence (PRBS) parameter identification

Previous work in analysis of batteries has demonstrated a frequency domain approach, using pseudo random binary sequences (PRBSs), facilitates parameter identification [18–20].

PRBS generators can be realised using shift registers with modulo 2 (XOR) feedback, Fig. 3, at predetermined "tap" positions [21].

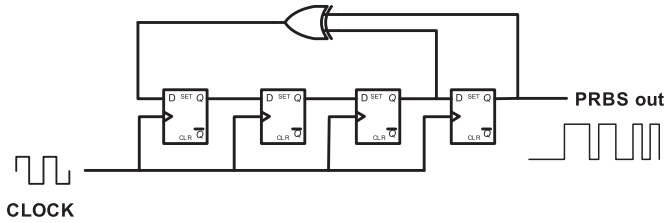

Fig. 3. 4-Bit PRBS generator example.

Fig. 3 shows a 4-bit PRBS generator. For the work described here, a software implementation of the PRBS is carried out.

3. Test system description

The test equipment comprises a data acquisition system, running proprietary software acquiring data from two measurement channels (Fig. 4). Battery terminal voltage and battery current data are captured. The bandwidth of the system allows sampling at 2.5 kHz with this number of inputs with a measurement resolution of 16 bits, 20 V FSD, allowing 0.3 mV resolution of the battery terminal voltage.

The test system comprises three separate loading elements for carrying out the tests. A Kikusui 300 W electronic load, pre-set for constant current discharge, is used for pulse testing, and is additionally connected to the output of the VxI Power Ltd, Oracle 200 W intelligent charger [22], which functions as a DC Uninterruptable Power Supply (UPS). This allows discharge of the battery via the unit into the external load, with the VxI unit controlling its own deep discharge disconnection, to protect the battery at the end of the test. The second load is integral to the VxI unit, in the form of an on board constant current load, which is controlled by the on board microcontroller to provide a 2 pulse test, allowing voltage deviations of the connected battery to be established.

Thirdly, a high speed load is incorporated, which is subjected to perturbations by the PRBS generator, realised in a Microchip PIC development board.

Finally, temperature compensated charging is provided by the VxI charger prior to tests, the unit sensing battery temperature directly, and modifying charge voltage for prevailing temperature.

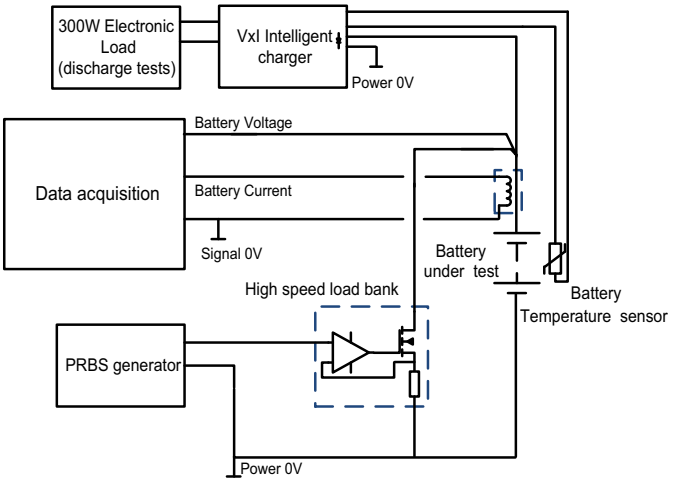

Fig. 4. Test system block diagram, conventional lead-acid and UltraBattery™ tests.

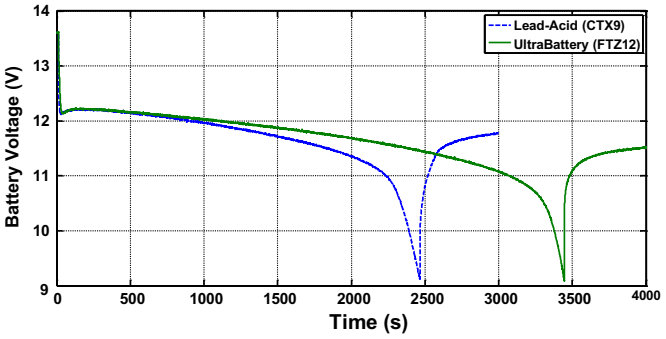

Fig. 5. 1 C discharge, 20 °C, both batteries.

3.1. Test procedure

3.1.1. Discharge tests

The test batteries used were a conventional generic lead-acid battery (CTX9-12) for starting lighting and ignition rated at 12 V, 8 Ah, and a comparably sized UltraBattery™ (Furukawa FTZ12-HEV) rated at 12 V, 8.5 Ah.

Initially, discharge tests were carried out on the two batteries, at a rate around 1 C (8 A) to compare capacity.

The test was carried out using the VxI battery backed power supply, in its "AC fail mode". The low voltage cut-off of the unit was set deliberately low at 9.2 V, in order that the complete discharge could be seen.

Fig. 5 shows the discharge curves for the batteries at the 1 C rate, 20 °C. A further test at the same discharge rate in a −20 °C ambient was carried out to establish low temperature performance (Fig. 6). Detailed manufacturer's data was not available for the batteries under test regarding end-of-discharge voltage for associated discharge rate, so generic guidelines from Yuasa were used [23]. (The Yuasa NP manual represents some of the most detailed application data for VRLA batteries, and is useful as a general guide for non-Yuasa types.) The capacities for both batteries during the tests, along with values for C_{Bulk}, calculated based on the discharges at room temperature are shown in Table 1.

Interesting to note is that at 20 °C the UltraBattery™ has almost 30% more capacity than the conventional battery. However, at −20 °C the two batteries only show a difference of around 10%. This may indicate that the parallel capacitor structure of the battery leads to some reduction in capacity at low temperature, although further testing would be required to verify this.

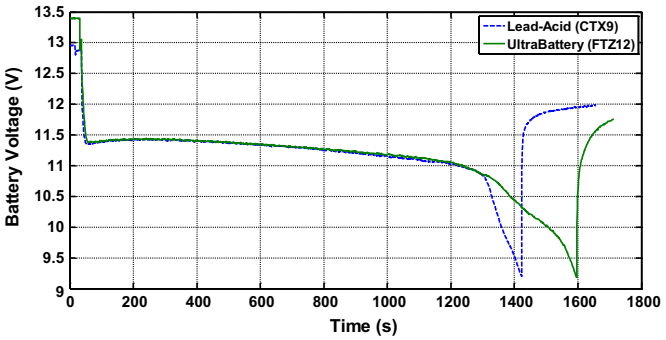

Fig. 6. 1 C discharge, −20 °C, both batteries.

Table 1
Discharge test results.

Battery	Discharge time (s)	Capacity ((Ah)	Capacitance (F)
20 °C Test			
Conventional (CTX9)	2451	5.45	7561
Ultra battery (FTZ12)	3433	7.63	10,586
−20 °C test			
Conventional (CTX9)	1415	3.14	–
Ultra battery (FTZ12)	1588	3.5	–

3.1.2. Two pulse battery tests

The use of two pulse battery testing has been present in VxI Power battery backed power supplies since 2001, and has been independently described in the work of Coleman et al. [16]. The purpose of the test is to establish state of health of the battery by applying a load pulse. The test is conditional on the battery being fully charged. The purpose of the dual pulse is to place the battery into a predictable terminal voltage condition before the test pulse and measurement is applied. Figs. 7 and 8 show the conventional and UltraBattery™ tests respectively.

Referring to Fig. 7, an explanation of the test is as follows: At position (A) the charger is disabled and the battery is effectively open circuit. At (B) the first load pulse is applied, which "clips" the battery terminal voltage to a steady-state level, seen during the "relax" period (C). A measurement is taken at (D) just before the second test pulse is applied, a further measurement being taken at (E). The voltage deviation (D–E) is calculated and this is the test result. Finally at (F) we see the charger enabled once more and the battery voltage rising to the float voltage.

Results of the two pulse test are shown in Table 2.

The results of the tests in isolation only report the batteries are in a good state of health (a typical fail limit in a commercial DC UPS for a 7 Ah battery, with headroom allowed for low temperature operation, would be in the order of 700 mV). However, the response of both batteries to the initial pulse is interesting. The UltraBattery™ showed a much smaller reduction in terminal voltage with the applied pulse load, which is anticipated to be due to the integral capacitor.

3.1.3. Static parameter evaluation

The batteries were subject to static load pulses initially in order to establish the parameters for the Randles' circuit (Fig. 9).

The static tests gave rise to results which were as expected generally, with the UltraBattery™ being lower in impedance by around 30%. However, inspection of the responses proved difficult overall, and distinguishing R_i from R_t particularly difficult, making $C_{Surface}$ difficult to report accurately. As such the total of $R_i + R_t$ was recorded as a reference for the later PRBS tests (Table 3).

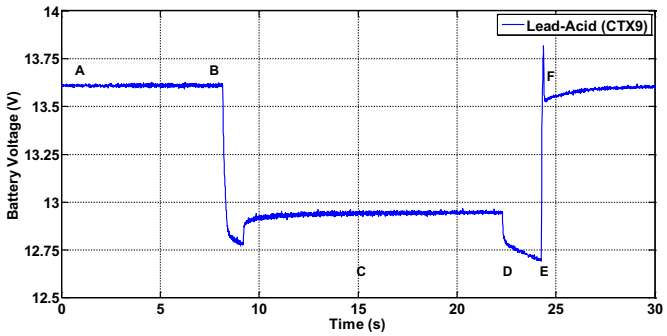

Fig. 7. Lead-acid two pulse battery test.

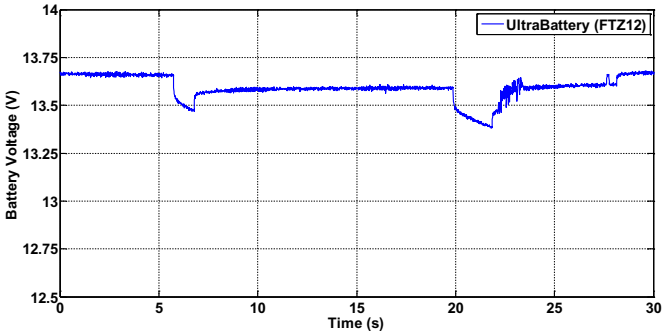

Fig. 8. UltraBattery™ two pulse battery test.

3.1.4. PRBS battery testing

Using PRBS to evaluate the impedance spectra of batteries, a constant current load of a known magnitude is applied, driven by the PRBS and the subsequent voltage disturbance observed at the battery terminals. FFTs of both current and voltage are obtained which lead to impedance spectra for the battery under test.

The impedance plots were compared to simulations based on the Randles' model. A fit was established for the conventional battery (Fig. 10).

The UltraBattery™ however proved more difficult, as the response obtained did not fit the Randles' simulation, indicating a revision was required to the model. Inspection of the response tended to indicate a capacitance was shunting the series $C_{Surface}$ and C_{Bulk} networks in the Randles' circuit, and making an assumption that the anomaly was due to the battery effectively containing a parallel capacitive element, a new model was developed taking this into account. Examining the frequency range of this effect (10 Hz down to 1×10^{-2} Hz), it was estimated at this capacitance being in the 50–200 F range, with a small series impedance (Fig. 11).

Using an iterative approach, parameters were established for the simulation model which provided a good fit to the experimental results. The experimental results, compared to the model simulation are shown in Fig. 12.

To close off the investigation, the modified model was applied to the conventional battery, to see if the fit was improved. Using approximate values as a starting point, an improved fit was established, which can be seen in Fig. 13.

It was therefore concluded that the revised model offered benefits to establishing parameters for both batteries. A summary of the established parameters is found in Table 4.

3.1.5. Results summary

3.1.5.1. Battery mass. The batteries were weighed for completeness, bearing in mind the UltraBattery™ is designed for HEV usage (Table 5).

4. Testing of parallel energy storage networks

The findings of the tests comparing the UltraBattery™ to the conventional lead-acid battery, gave rise to questions regarding the modified model, and the respective roles of the capacitor and

Table 2
Two pulse battery test results.

Battery	Measured deviation
Conventional (CTX9)	250 mV
Ultra battery (FTZ12)	210 mV

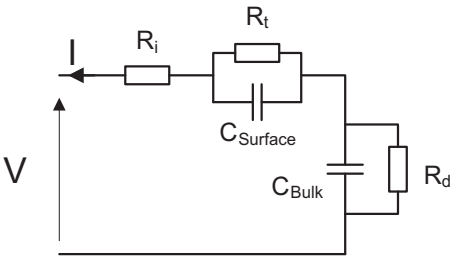

Fig. 9. Randles' equivalent circuit.

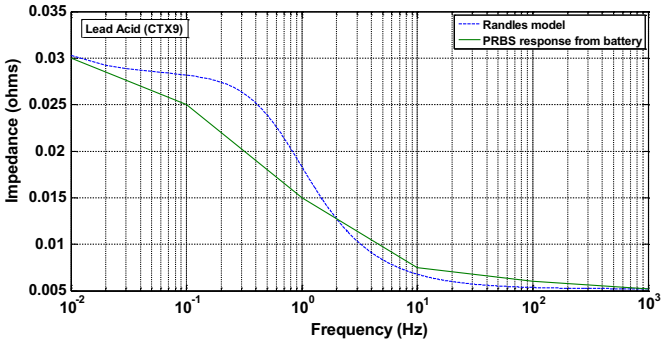

Fig. 10. Impedance response (experimental) for lead-acid battery compared to simulation.

battery in a parallel combination. As such, an experiment was devised to characterise battery/supercapacitor parallel combination in an attempt to investigate further the improvement offered by the high-carbon technique.

The capacitor banks chosen were significantly different in order to inform the model already developed for the UltraBattery™.

4.1. Test battery configurations – battery with parallel supercapacitor bank

4.1.1. Supercapacitor bank 1

The supercapacitors used were Wima DS-C-09-01-C200-XB-M-SS rated at 200 F, 2.5 V DC. In order to achieve the terminal voltage of the battery, capacitors connected in series were used to increase the working voltage. This in turn reduced the overall capacitance by the same factor, resulting in a bank 1/6 of the rated capacitance value per capacitor.

4.1.2. Supercapacitor bank 2

The second capacitor bank again used 6 capacitors connected in series, but of higher capacitance. The capacitors used were Maxwell Energy Products PC 2500, of value 2500 F, 2.7 V. The total capacitance was therefore (calculated) 417 F.

4.2. Capacitance tests

All commercial capacitors are manufactured with a wide capacitance tolerance, so charge and discharge tests of the bank were carried out in order to establish the actual capacitance experimentally.

The capacitors were charged to a terminal voltage of 15 V using a constant current of 2 A. Subsequently the pack was discharged using a constant current 2 A load.

Calculations of stored charge (Coulombs) were then carried out in order to establish capacitance values (Table 6).

4.3. Test system description – parallel network PRBS tests

The test system used in the earlier tests was modified with the addition of further input from a total of five channels of measurement (Fig. 14). The channels consist of battery terminal voltage, an offset measurement to determine any voltage dropped in the system wiring, 3 channels of current measurement (capacitor current, battery current and total current).

Table 3
Randles' parameters (from static tests).

Battery	$R_i + R_t$
Conventional (CTX9)	31 mΩ
Ultra battery (FTZ12)	21.25 mΩ

Fig. 15 shows the test system photograph. To the left of the picture the data acquisition system is seen, and referring to the aerial view in Fig. 16 we can see the parallel connection of the battery and the smaller supercapacitor bank.

Fig. 17 shows more detail of the test system with capacitor bank 2. (The twisted wires from the charger to battery are the temperature sensor for the battery temperature compensation.)

4.4. PRBS application to the energy storage network under test

Using PRBS testing to evaluate batteries, a constant current load of a known magnitude is applied, driven by the PRBS and the subsequent voltage disturbance observed at the battery terminals. FFTs of both current and voltage are obtained which lead to impedance spectra for the battery under test.

Tests on the capacitor/battery parallel combination are carried out in the same way, using the conventional battery (CTX9) in parallel with a supercapacitor network. During these tests additional information is gathered regarding the current profiles. Current measurement is carried out on each circuit leg, in addition to the total current flowing in the load. Analysis of these current responses is carried out in order to gain insight into the range of frequencies over which the supercapacitor offers performance improvements over the battery alone.

4.5. Test results

Prior to carrying out frequency domain analysis of the acquired data, the data was plotted in order to allow inspection of the waveforms.

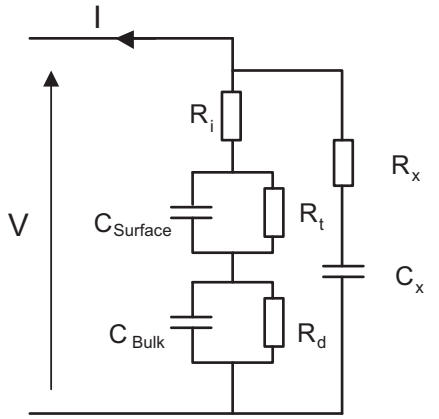

Fig. 11. Modified Randles' model for the UltraBattery™.

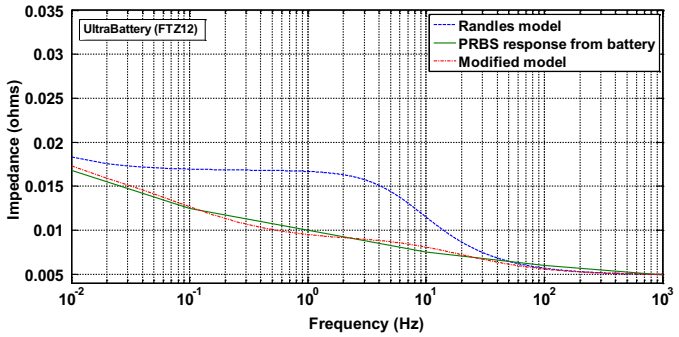

Fig. 12. UltraBattery™ experimental response and simulation using modified model.

Prior to the test the battery/capacitor combination was charged at a cyclic charge level [23] (2.4 V per Cell (VpC) at 20 °C), as this was considered to be closer to the conditions under which the parallel combination would be used in application, rather than as a standby power source. The PRBS perturbations as applied to the test configurations were used not only to establish impedances, but the voltage and current waveforms were inspected to attempt to gain information regarding the respective roles of the two energy stores. Lead-acid batteries, on transition from charge to discharge, experience a steep reduction in terminal voltage, and it has been observed in earlier work [18] that a voltage level of around 2.03 VpC at 20 °C (12.2 V for a 12 V battery) represents a pseudo steady state during early discharge, and this voltage is seen to be significant in the discharge of parallel network. Figs. 18–28 which follow show the results obtained.

4.5.1. Test waveforms – battery and capacitor banks

Fig. 18 shows the overall current envelope for the 33 F capacitor and the test battery. As can be seen the current sharing between the two elements reaches a pseudo steady state at just over 200 s. Fig. 19 shows the comparable response for the battery in parallel with the 417 F capacitance. In this figure the role of the capacitor is much more significant in delivery of current over the test duration. The corresponding voltage responses for the two networks can be seen in Fig. 20:

The voltage response for the battery/33 F network shows a similar characteristic to a battery without capacitor, the main difference being the gradient of the section for 0–200 s, which has a reduced gradient due to the additional energy stored in the capacitor bank. In contrast for the battery/417 F network, the voltage response is almost linear up to 900 S where the terminal voltage of the pair reaches a pseudo steady-state level.

Examining the current waveforms in more detail, the initial 100 s of the battery/33 F network response are shown in Fig. 21. The capacitor delivers the majority of the current, and over the course of the plot this reduces as the capacitor discharges relative to the battery voltage.

The corresponding results for the larger capacitor are presented in Fig. 22. Battery current is almost negligible during this period. Pulse by pulse voltage deviations (Fig. 23.) are less than 50% of those seen with the smaller capacitor bank.

The battery/33 F begins a transition in the relative currents of the network components at around 100 s. Fig. 24 shows that the relative currents have started to move towards equalisation, indicating the chemical reactions within the battery have started to proceed.

The corresponding transition for the battery/417 F bank occurs around 800–900 S (Fig. 25), however the capacitor continues to supply the bulk of the current beyond this time.

Later in the test (1000–1100 s, Fig. 26), the battery is now supplying the bulk of the current for the 33 F network, whilst charging the capacitor in the off period. However, the average level of ripple current seen by the battery is still much reduced by the addition of the capacitor.

The corresponding waveforms over the same test period for the battery/417 F bank are shown in Fig. 27. The network has moved to a pseudo steady state in terms of the respective current sharing, but the effect of the larger capacitance remains apparent with the lower battery ripple current observed.

The voltage responses during this time are shown in Fig. 28. The ripple voltage of the two networks is further indicative of the role of the capacitor in delivering current in transient load conditions.

4.5.2. Battery impedance (PRBS tests)

The test arrangement dictated that addition of the current sensing elements for both the capacitor and battery introduced

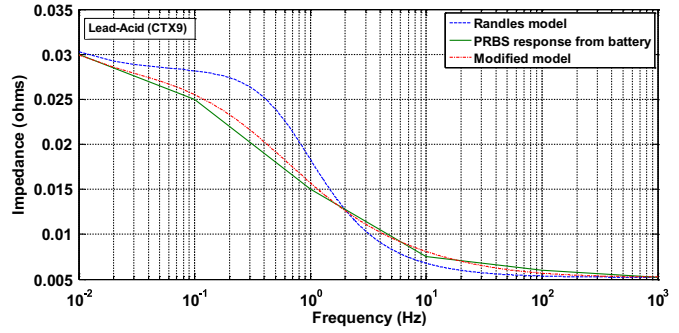

Fig. 13. Lead-acid experimental response and improved fit to modified model.

Table 4
Battery parameters.

Randles' model				
	R_i (mΩ)	R_t (mΩ)	$C_{Surface}$ (F)	C_{Bulk} (F)
CTX	5.2	23	2	7561.3
FTZ	4.9	11.9	3	10,586

Modified model						
	R_i (mΩ)	R_t (mΩ)	$C_{Surface}$ (F)	C_{Bulk} (F)	C_x (F)	R_x (mΩ)
CTX	5.2	23	2	7561.3	10	6
FTZ	4.9	11.9	2.5	10,586	100	6

Table 5
Battery mass.

Battery	Mass (kg)
Conventional (CTX9)	2.85
Ultra battery (FTZ12)	3.75

Table 6
Capacitance values, supercapacitor banks.

Bank 1 charge	**Bank 1 discharge**
$Q = 658$ C	$Q = 652$ C
$C = 47.0$ F	$C = 46.6$ F
Bank 2 charge	**Bank 2 discharge**
$Q = 8960$ C	$Q = 7152$ C
$C = 601.3$ F	$C = 510.86$ F

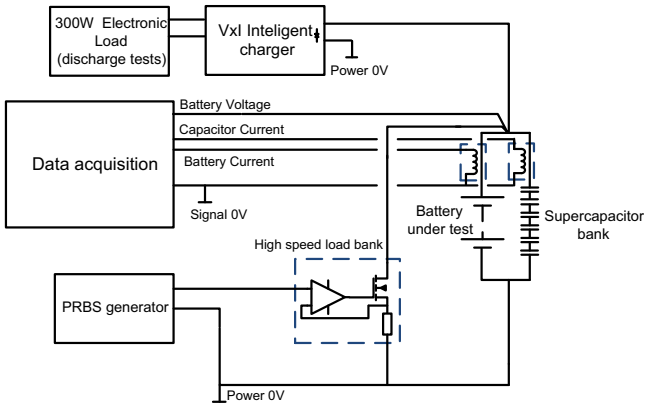

Fig. 14. Test system block diagram, parallel network tests.

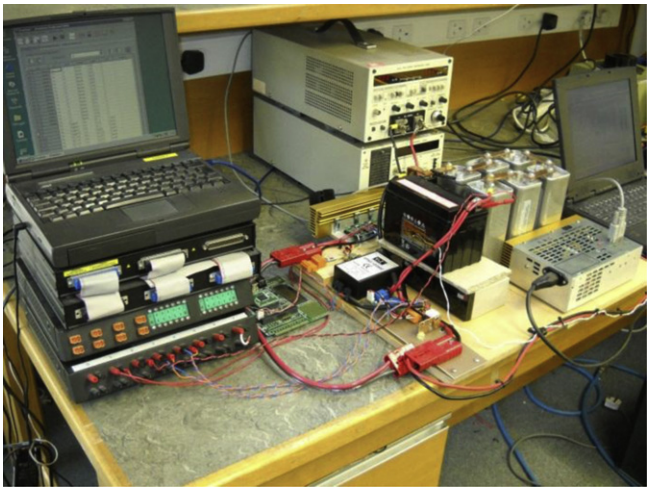

Fig. 15. Test system photograph.

additional impedance into the test setup. As part of the test, a differential voltage measurement was carried out in order to establish this impedance so it could be subtracted from the overall results. PRBS impedance results were obtained for the batteries and

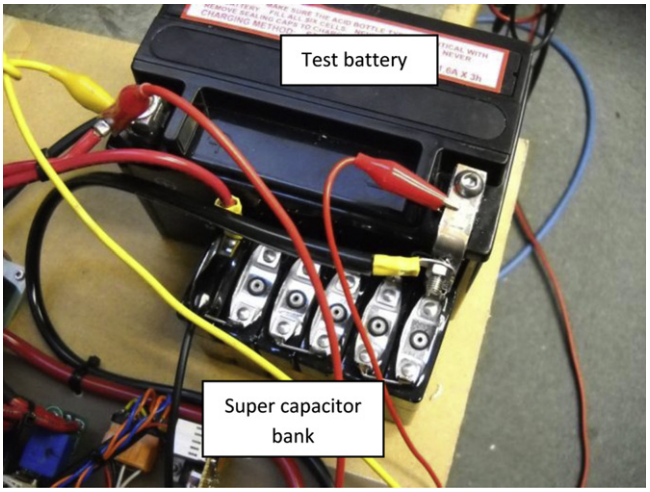

Fig. 16. Battery/supercapacitor test setup, bank 1.

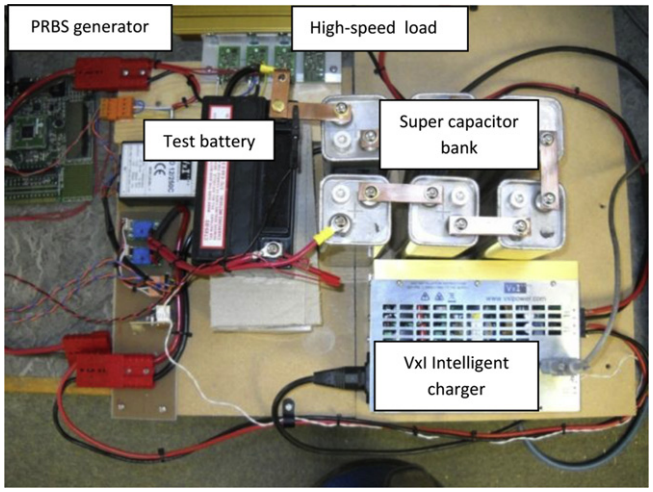

Fig. 17. Battery/supercapacitor test setup, bank 2.

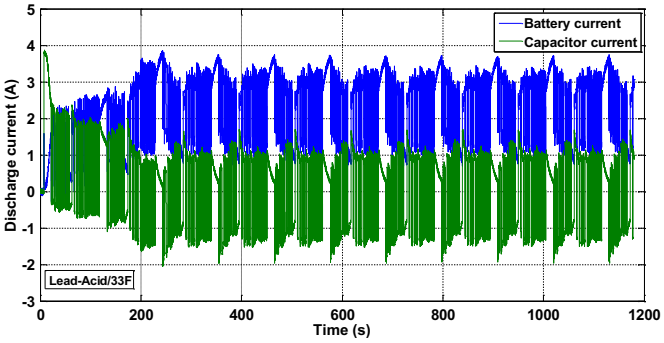

Fig. 18. Relationship between battery and capacitor current over full test – bank 1.

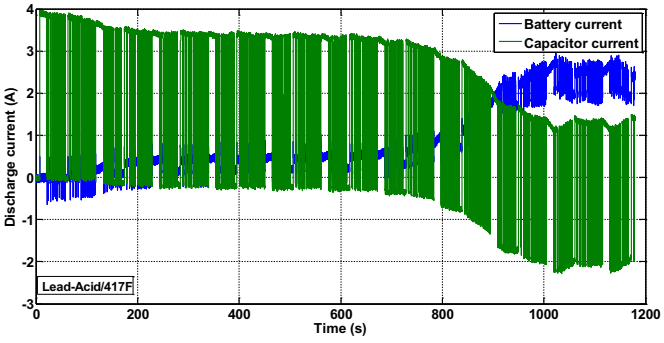

Fig. 19. Relationship between battery and capacitor current over full test – bank 2.

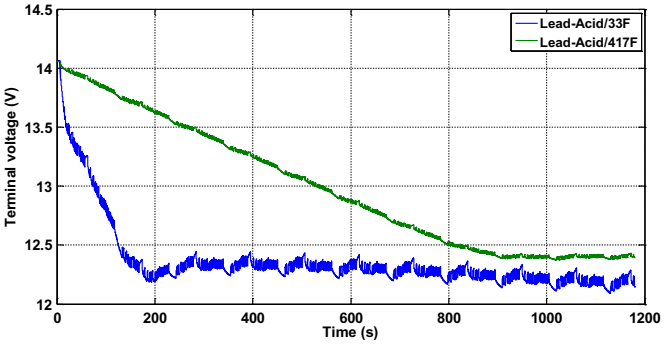

Fig. 20. Terminal voltage of both parallel networks over the full test period.

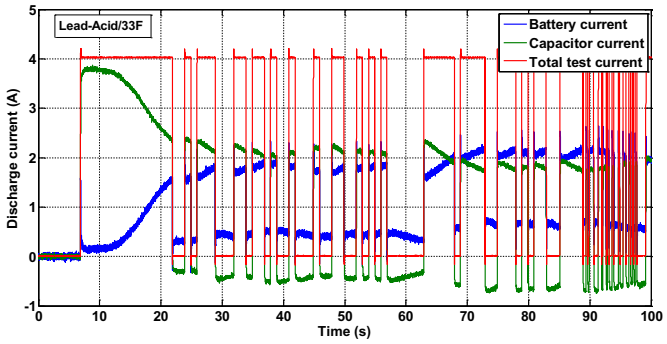

Fig. 21. Capacitor, battery and total test current, bank 1 (0–100 s).

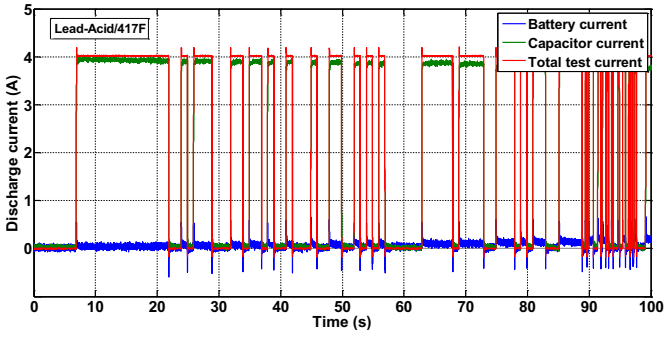

Fig. 22. Current waveforms during test, bank 2 (0–100 s).

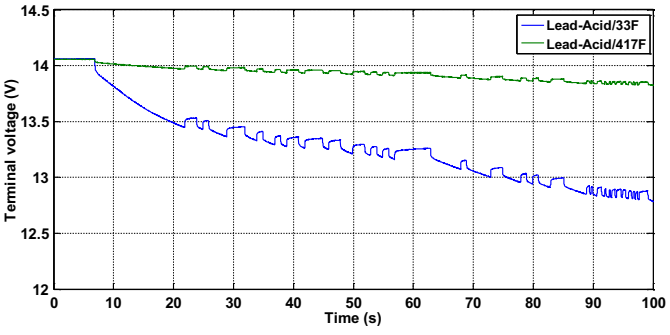

Fig. 23. Terminal voltage of both parallel networks 0–100 s.

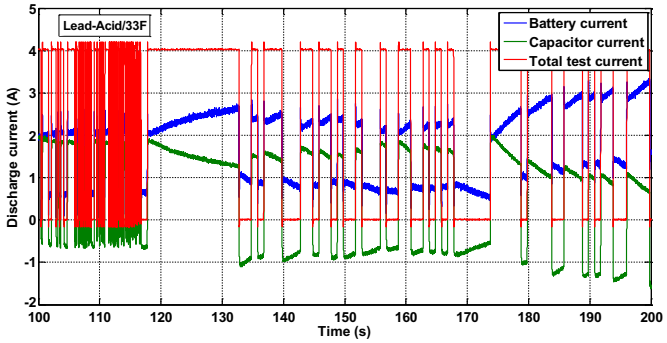

Fig. 24. Capacitor, battery and total test current, 100–200 s, bank 1.

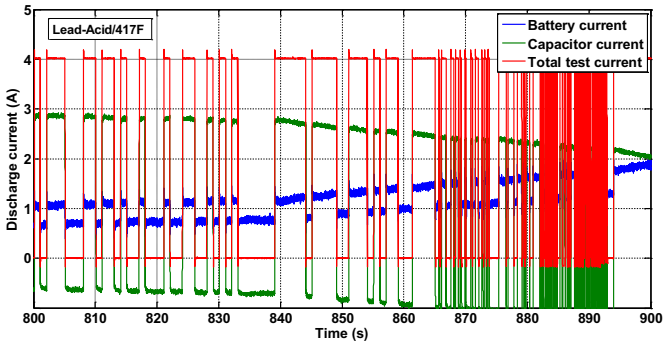

Fig. 25. Discharge current with battery terminal voltage, bank 2 (800–900 s).

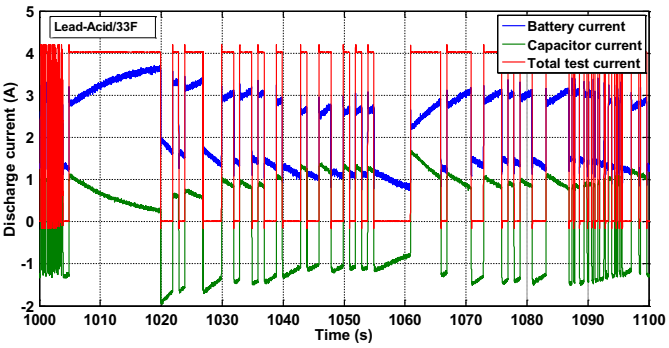

Fig. 26. Capacitor, battery and total test current, 1000–1100 s, bank 1.

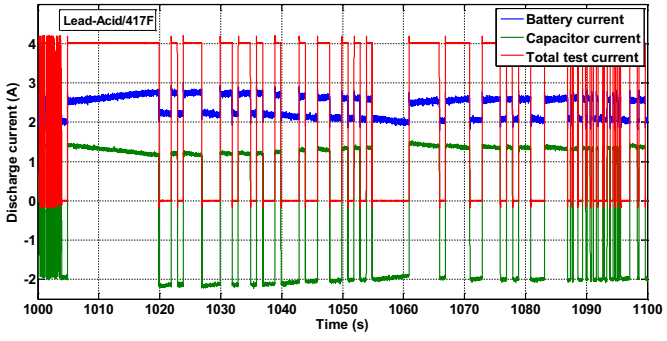

Fig. 27. Current waveforms during test, 1000–1100 s, bank 2.

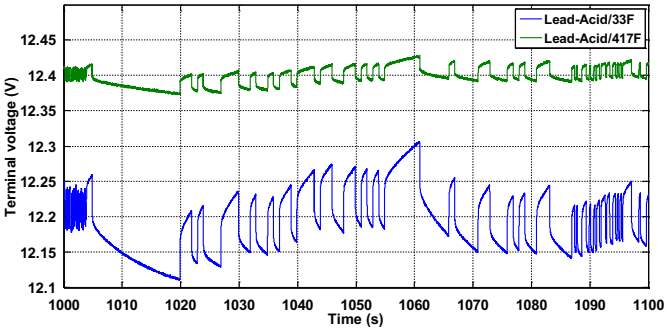

Fig. 28. Terminal voltage of both parallel networks 1000–1100 s.

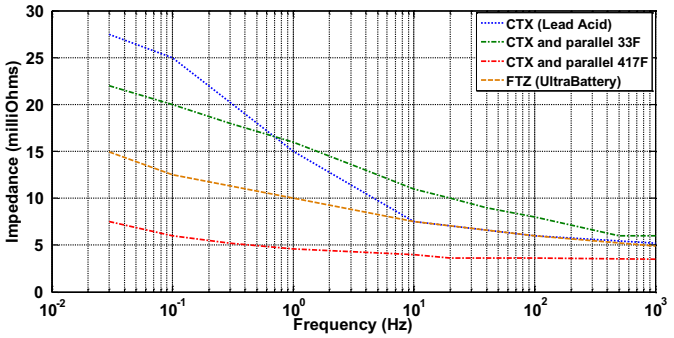

Fig. 29. Respective impedances of the battery and parallel networks.

parallel combinations in pseudo steady-state conditions, and are shown in Fig. 29.

Examination of the results (Fig. 29), bears out the predictions of the earlier tests with the batteries alone. The conventional battery was shown in Section 2 to have significantly larger impedance than the UltraBattery™ over the frequency range and in addition to this the UltraBattery™ response was observed to be significantly flattened by the shunting effect of the parallel capacitance. The predictions for the UltraBattery™ using curve fitting suggested a parallel capacitance of circa 100 F. The responses in Fig. 29 support the earlier calculations, with the high-carbon response lying between the two parallel configurations (33 F and 417 F).

5. Conclusion

Examination of the UltraBattery™ against its conventional counterpart revealed improvements in performance using the conventional tests, mainly related to Ah capacity and overall internal impedance. Interestingly, however, when subjected to the VxI pulse tests, the level of terminal voltage clipping by the preload pulse was much reduced for the UltraBattery™, indicating the additional capacitance able to support short duration discharges. Examination of the response obtained by PRBS identification let to the development of a modified Randles' model which provided a good fit to the UltraBattery™ results. Using the proposed model the difference between the two battery types became clear, with a 10:1 difference in the capacitance value C_x which was the significant performance indicator.

The UltraBattery™ was considerably heavier than the conventional type, raising questions regarding its application in HEVs. This area requires further investigation, as the weight penalty may not be solely due to the integral additional capacitance, and there may be other performance benefits which have not been highlighted within this work.

The results obtained by the earlier tests gave rise to further investigations using the conventional battery and parallel supercapacitors. Using the two chosen test capacitances a reduction in overall impedance was observed when both configurations were subjected to frequency domain analysis. This was in line with the tests carried out with the UltraBattery™, which incorporates the capacitor within the battery structure. Parallel capacitances of 33 F (47 F measured) and 417 F (510 F measured) were shown to produce responses which, when compared to the 100 F calculated parallel capacitance of the UltraBattery™, confirmed the earlier results.

Analysis of the current flows within the parallel combination offered some insight into the mechanisms at work within the high-carbon types. The examination showed clearly that during the early stages of load application, the supercapacitor delivers current, whilst the battery begins to undertake the chemical processes that allow discharge. The relationship between the current delivered by each energy store is dependent on the magnitude of the parallel capacitance and prevailing dynamic loading, and changes as time progresses. Ripple currents seen by the battery are significantly reduced using the parallel arrangement throughout the discharge, leading to extended service life by reduction of heating effects and gassing and also by some extent the number of charge/discharge cycles the battery experiences.

Examination of the voltage responses, respective current flows and ripple currents offer opportunities for further work in defining criteria for selecting parallel capacitors in applications where transient conditions are the norm. Furthermore, the knowledge gained from the model of the UltraBattery™ allows the suitability for its use in potential applications by simulation or experiment using the discharge profiles for the target application. Respective current flows between the parallel components would allow some evaluation of the predicted performance using the UltraBattery™, thus justifying the investigations carried out.

Issues remain with the working voltage of available supercapacitors when applied in a parallel configuration with a VRLA battery. Cell/capacitor parallel configurations are suited to the typical working voltages of 2.5–2.7 V, but a series combination of capacitors is required to operate when batteries are used at higher terminal voltage levels. Close monitoring of the individual capacitor voltages during the tests was carried out to ensure the deviation between capacitors did not become an issue. In application, active balancing would need to be used for supercapacitor/battery parallel operation, adding complexity and cost and reducing efficiency. The UltraBattery™ avoids these issues with the supercapacitor being integral to the battery chemistry.

However, discharge of the battery is limited by the minimum end cell terminal voltage, which is defined by load current, but can generally be regarded as being 1.67 V per Cell (VpC) at 20 °C. In contrast, capacitors can be discharged to zero terminal voltage with no ill effects. This in itself highlights a limitation placed on the use of a parallel capacitor by its connected battery – when the battery has discharged to its end cell terminal voltage, the capacitor will have unused energy which cannot be accessed whilst remaining in parallel with the battery.

As discussed, the observed reduction in battery ripple current in the supercapacitor/battery parallel combination is a significant factor in improving battery service life. The mechanism of this current sharing within the UltraBattery™ may lead to improvements in service life of these types of storage device, but further information regarding the chemical implementation of the capacitor in these battery types would be needed to further quantify this.

Examinations of current waveforms during the tests were concerned only with those observed during the PRBS load pulses, and opportunities exist to investigate the effects of dynamic charge/discharge cycles on the parallel energy storage arrangement.

References

[1] W. Peukert, Elektrotechnische Zeitschrift. 20 (1897).
[2] B.E. Conway, Electrochemical Supercapacitors: Scientific Fundamentals and Technological Applications, Plenum Press, New York, 1999.
[3] Q. Liyan, Q. Wei, IEEE Transactions on Industry Applications 47 (2011) 359–367.
[4] J.M. Miller, in: Power Electronics, 2007. ICPE '07. 7th International Conference on, 2007, pp. 16–22.
[5] P. Serp, J.L. Figueiredo, Carbon Materials for Catalysis, John Wiley & Sons, Hoboken, N.J., 2009.
[6] P.M. Gregory, H. Qingyuan, Nanotechnology 20 (2009) 204023.
[7] D. Pavlov, P. Nikolov, T. Rogachev, Journal of Power Sources 196 (2011) 5155–5167.
[8] D. Pavlov, T. Rogachev, P. Nikolov, G. Petkova, Journal of Power Sources 191 (2009) 58–75.
[9] P.T. Moseley, R.F. Nelson, A.F. Hollenkamp, Journal of Power Sources 157 (2006) 3–10.

[10] L.T. Lam, R. Louey, Journal of Power Sources 158 (2006) 1140–1148.
[11] J. Furukawa, T. Takada, D. Monma, L.T. Lam, Journal of Power Sources 195 (2010) 1241–1245.
[12] A. Cooper, J. Furakawa, L. Lam, M. Kellaway, Journal of Power Sources 188 (2009) 642–649.
[13] D. Linden, Handbook of Batteries, second ed., McGraw-Hill, New York, 1995.
[14] E. Barsoukov, J.R. Macdonald, Impedance Spectroscopy: Theory, Experiment, and Applications, second ed., Wiley-Interscience, Hoboken, N.J./Chichester, 2005.
[15] A.J. Fairweather, M.P. Foster, D.A. Stone, Journal of Power Sources 207 (2012) 56–59.
[16] M. Coleman, W.G. Hurley, L. Chin Kwan, IEEE Transactions on Energy Conversion 23 (2008) 708–713.
[17] B.S. Bhangu, P. Bentley, D.A. Stone, C.M. Bingham, IEEE Transactions on Vehicular Technology 54 (2005) 783–794.
[18] A.J. Fairweather, M.P. Foster, D.A. Stone, in: IET Conference Publications, 2010, TU244.
[19] A.J. Fairweather, M.P. Foster, D.A. Stone, in: Evs 25 WEVA No. 4, Shenzhen, China, 2010, p. 405.
[20] A.J. Fairweather, M.P. Foster, D.A. Stone, Journal of Power Sources 196 (2011) 9398–9406.
[21] W.D.T. Davies, System Identification for Self-Adaptive Control, Wiley-Interscience, London, New York, 1970.
[22] VxI Power Ltd, in: VxI Power Ltd, Lincoln, 2012, Oracle 200E product webpage.
[23] Yuasa Battery Europe, in: NP VRLA Application Manual, Yuasa Battery Corporation, 1999. pp. 1, 2, 5, 6, 7, 8, 9, 12, 22, 24, 27, 29.